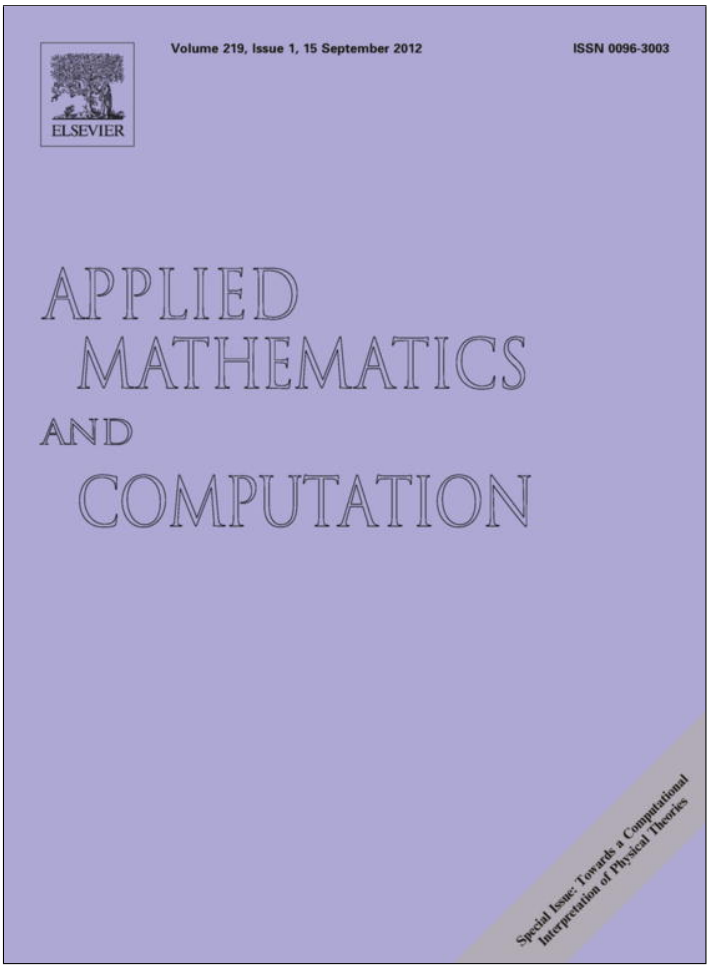

Applied Mathematics and Computation 219 (2012) 376–388

Contents lists available at SciVerse ScienceDirect

Applied Mathematics and Computation

journal homepage: www.elsevier.com/locate/amc

Asymptotic, numerical and approximate techniques for a free boundary problem arising in the diffusion of glassy polymers

S.L. Mitchell *, S.B.G. O'Brien

Mathematics Applications Consortium for Science and Industry (MACSI), Department of Mathematics and Statistics, University of Limerick, Limerick, Ireland

ARTICLE INFO

Keywords:
Controlled drug release
Solvent penetration
Asymptotics
Boundary immobilisation
Stefan problem
Keller box scheme
Heat balance integral method
Artificial parameter

ABSTRACT

This paper considers approximate solution methods for a one dimensional Stefan problem describing solvent diffusion in glassy polymers. Similar to the classic Stefan problem, the region initially has zero thickness and so must be analysed carefully before performing a numerical computation. A small-time analysis gives the correct starting solution which is then incorporated into the second order accurate Keller box finite difference scheme. We also consider a detailed analysis of small and large time expansions, as well as the large control parameter limit, and show that our generalised approach enables us to obtain higher order terms than given in previous studies. Finally, we apply the combined integral method (CIM) to this problem, which is a refinement of the popular heat balance integral method (HBIM), and compare both the CIM and asymptotic solutions to the numerical results.

1. Introduction

An important problem in the pharmaceutical industry is the role of solvent diffusion in polymer systems as this greatly affects drug delivery processes. Mathematical models plays a useful role in illustrating the drug release mechanisms involved and can therefore help in the development of new pharmaceutical products. These models can provide insights into the effect of design parameters on the drug release mechanism, such as device geometry and drug loading. Drug-polymer systems can also be used to protect the drug from biological degradation prior to its release. A comprehensive review of models for solvent penetration in polymers can be found in [3].

The drug release mechanism from a polymer matrix is usually categorised as a diffusive process [9]. The drugs are either released by diffusion alone or by diffusion combined with other physical mechanisms [3,7]. In this study we are interested in a mathematical model where the glassy-rubbery interface is described by a moving boundary whose kinetics is governed by an empirical law that relates the concentration of solvent at that point to the velocity of the interface, as discussed in [2,4,7,8,13,17] and references therein. It can be thought of as a Stefan problem [10], which usually describes the melting or solidification of a material, and these occur in a wide variety of natural and industrial applications. Mathematically, these problems represent a particular kind of non-linear boundary value problem where the phase-change boundary moves with time, and its location is not known in advance. The model for diffusion in glassy polymers studied here can also be applied to a one-phase Stefan problem which is generalized to include kinetic undercooling at the moving boundary [12]. The kinetic condition relates interface undercooling to interface growth rate which is characterised by a dependence of the phase-change temperature on the velocity of the phase-change boundary.

* Corresponding author.
E-mail address: sarah.mitchell@ul.ie (S.L. Mitchell).

0096-3003/$ - see front matter © 2012 Elsevier Inc. All rights reserved.
http://dx.doi.org/10.1016/j.amc.2012.06.026

In this paper we consider the one-dimensional free boundary problem describing a glassy polymer and penetrant as described in [7], and analyse how to predict and control the diffusive behaviour of the penetrant into the polymer. Similar to the classic Stefan problem describing the freezing of a mass of liquid, the region initially has zero thickness and so must be analysed carefully before performing a numerical computation [23]. We follow this approach and use a small-time analysis, along with a transformation to immobilize the boundary, to find the correct starting solution. The fully implicit Keller box finite-difference scheme is then applied to the model, which is second order accurate in time and space [23,24]. Abd-El-Salam and Shehata [1] also consider an implicit finite difference scheme for the same problem but they do not correctly obtain a starting solution and their scheme is less compact than the box scheme, which only uses two neighbouring values at each time and spatial step. In addition, the box scheme requires the model to be re-formulated as a first order system and this leads to second order accuracy for the flux variable as well as the concentration and moving boundary variables.

Several authors have considered asymptotic limits of small and large time as well as large control parameter, for example a large Stefan number, both for this problem and the kinetic under-cooling problem [7,12,17]. We give a detailed analysis of these limits, obtaining terms that have not previously been found and compare these solutions to the numerical results. In addition, we consider a further expansion in the large parameter limit and we demonstrate that the resulting expansions are robust even for values not much above $\mathcal{O}(1)$. Previous authors consider small and large time expansions after having applied a transformation to immobilise the boundary [7,12]. For the small time solution they use the unknown moving boundary as the expansion parameter which leads to having to solve a non-linear equation for this parameter after finding the approximate solution at different orders. We show that a systematic approach can be applied to the original formulation for the three different limits, allowing new higher order terms to be determined directly.

We also describe the heat balance integral method (HBIM), which is a popular approximate solution technique for solving thermal problems [14,20], and apply it to the diffusion polymer model. In the case of the classic Stefan problem describing a melting or solidification process, the method involves assuming an approximating function for the temperature, typically a polynomial, and then integrating the heat equation over the spatial domain. This reduces the problem to solving a set of first order ODEs, which often have analytic solutions. For the diffusion polymer model we can define an approximating function for the concentration in the same way, but there is an added complication of a non-zero phase-change concentration which means that the HBIM leads to a second order ODE for the moving boundary. However, this can easily be dealt with by using information from the small time analysis to deduce an extra initial condition. An alternative approach to the HBIM is the refined integral method (RIM), where the heat equation is integrated twice [20,28]. The relative merits of the two approaches are discussed in detail in [20]. Recently, Mitchell and Myers [21,27] have developed a method where the exponent in the approximating polynomial is determined during the solution process, producing significantly better results than previous heat balance methods. It involves a combination of the conventional heat balance and refined integral methods, and is called the combined integral method (CIM). Unfortunately, for large values of the control parameter, the resulting ODEs found from applying the CIM to this model turn out to be difficult to solve using a standard ODE solver in Matlab. We therefore use the large time analysis to obtain a limiting value for this exponent, and show that it gives very accurate results when compared to the numerical solution, in addition to being more accurate than the classic HBIM.

The layout of the paper is as follows. In Section 2 we formulate the governing equations describing the one-dimensional polymer diffusion model. A numerical method is given in Section 3, and we discuss a transformation to immobilise the boundary and perform an analysis in the small-time limit, which is necessary for the numerical solution. In Sections 4–6 we analyse the asymptotic limits of small and large time, and large control parameter, and compare these results with the numerical solution. In Section 7 we summarise the heat balance integral method and describe variants which make the method more accurate, and again show a comparison with the numerical solution. Finally in Section 8 we draw conclusions and discuss further extensions.

2. Mathematical formulation

Consider the problem where a slab of glassy polymer is in contact with a solvent [7]. If the solvent concentration exceeds some threshold value then the solvent moves into the polymer, creating a swollen layer in which the solvent diffuses according to Fick's second law of diffusion. The boundary between the swollen region and the glassy region obeys an empirical penetration law, relating its velocity to the solvent concentration at that point. An additional condition on the free boundary is obtained by imposing mass conservation, i.e., equating the mass density to the product of the solvent concentration and the velocity of the free boundary.

We assume that the swelling process occurs instantaneously at the penetration surface, the swollen region is at rest and the diffusivity D of the swollen polymer is constant. The problem can then be formulated as a one-phase free boundary problem for the concentration $u(x,t)$ of the penetrant and the unknown position $s(t)$ of the interface:

$$\frac{\partial u}{\partial t} = D\frac{\partial^2 u}{\partial x^2}, \quad 0 < x < s(t) \tag{1}$$

$$u = u_0 > u^*, \quad \text{at } x = 0 \tag{2}$$

$$(u + k_1)\frac{\mathrm{d}s}{\mathrm{d}t} = -D\frac{\partial u}{\partial x}, \quad \text{at } x = s(t) \tag{3}$$

$$\frac{ds}{dt} = k_2(u-u^*)^n, \quad \text{at } x = s(t) \tag{4}$$
$$s(0) = 0. \tag{5}$$

Eq. (1) is Fick's diffusion law for a one-dimensional system subject to a fixed concentration at $x = 0$, namely (2), where u_0 is the solubility of the solvent in the swollen polymer. The condition (4) is the penetration law describing the swelling kinetics, i.e., there is a threshold value u^* and above this value the interface moves with a speed given by a power law with index $n \geqslant 1$. Thus k_2 and n are phenomenological quantities. Finally, (3) gives the mass balance at the moving front. It is derived by assuming that the flux from the swelling region across the moving boundary, given by $-Du_x - us_t$ is proportional to the flux generated by the interface region. Thus

$$-D\frac{\partial u}{\partial x} - u\frac{ds}{dt} = K(u-u^*)^n, \quad \text{at } x = s(t),$$

and combining with (4) gives (3) where $k_1 = K/k_2$.

Previous work [1,2,4,7,8,13] does not explain the reason for allowing $n \neq 1$, apart from saying that the interface between the swollen and glassy region obeys an empirical penetration law. Most references only give results for $n = 1$, and Cohen and Goodhart [8] only use this value; hence to simplify the analysis, we assume that $n = 1$ henceforth. Indeed, McCue et al. [17] state that it is common to use a linear relationship in the kinetic law (4), with $n = 1$, and they use this value for most of their analysis. In addition, with $n = 1$ the model can be applied to the one-phase Stefan problem with kinetic undercooling [12].

The problem can be nondimensionalised by setting

$$x' = \frac{x}{X}, \quad t' = \frac{t}{T}, \quad u' = \frac{u-u^*}{\Delta u}, \quad s' = \frac{s}{X}, \tag{6}$$

where $\Delta u = u_0 - u^*$. Cohen and Erneux [7] choose X and T to balance the boundary conditions at $x = s$ which gives length- and time-scales as

$$X = \frac{D}{k_2(u^*+k_1)}, \quad T = \frac{D}{k_2^2(u^*+k_1)\Delta u},$$

with a parameter ϵ given by $\epsilon = \Delta u/(u^*+k_1)$. However, this formulation gives rise to an extra $\mathcal{O}(1)$ parameter in the diffusion equation. We therefore follow the more recent approach by Evans and King [12] and McCue et al. [17] and choose T to balance the diffusion equation. The simplest length-scale comes from balancing boundary condition (4) and so

$$X = \frac{D}{k_2\Delta u}, \quad T = \frac{X^2}{D} = \frac{D}{k_2^2\Delta u^2}. \tag{7}$$

Then Eqs. (1)–(5) simplify to (after dropping the $(\cdot)'$ notation)

$$\frac{\partial u}{\partial t} = \frac{\partial^2 u}{\partial x^2}, \quad 0 < x < s(t), \tag{8}$$
$$u = 1, \quad \text{at } x = 0, \tag{9}$$
$$(\lambda+u)\frac{ds}{dt} = -\frac{\partial u}{\partial x}, \quad \text{at } x = s(t), \tag{10}$$
$$\frac{ds}{dt} = u, \quad \text{at } x = s(t), \tag{11}$$
$$s(0) = 0, \tag{12}$$

where λ is a control parameter defined by

$$\lambda = \frac{u^*+k_1}{\Delta u} \tag{13}$$

and is $1/\epsilon$ in the model described in [7]. It is analogous to a Stefan number and typically varies from $\mathcal{O}(1)$ to large [17].

It should be noted that in Evans and King [12] they include a kinetic parameter μ in the boundary condition (11), so that it becomes

$$\mu\frac{ds}{dt} = u, \quad \text{at } x = s(t).$$

They set $\mu = \lambda$ which is equivalent to using the following length-scale

$$X = \frac{D}{k_2(u^*+k_1)}, \quad T = \frac{X^2}{D} = \frac{D}{k_2^2(u^*+k_1)},$$

rather than that defined in (7) above. The two models can easily be shown to be equivalent since applying the re-scaling $t = \lambda^2\hat{t}$, $x = \lambda\hat{x}$ and $s = \lambda\hat{s}$ to the Evans and King model leads to (8)–(12) for $u(\hat{x},\hat{t})$ and $\hat{s}(\hat{t})$. We find it more convenient to use the scalings in (7), which is equivalent to setting $\mu = 1$, because typically these parameters are not the same [17].

3. Numerical solution

For the numerical solution is it convenient to immobilise the boundary by setting

$$\xi = \frac{x}{s}, \quad u(x,t) = 1 + sF(\xi,t). \tag{14}$$

Then (8)–(11) become

$$ss_t F + s^2 \frac{\partial F}{\partial t} - \xi s s_t \frac{\partial F}{\partial \xi} = \frac{\partial^2 F}{\partial \xi^2}, \quad 0 < \xi < 1, \tag{15}$$

$$F = 0, \quad \text{at } \xi = 0, \tag{16}$$

$$(\lambda + 1 + sF)\frac{\mathrm{d}s}{\mathrm{d}t} = -\frac{\partial F}{\partial \xi}, \quad \text{at } \xi = 1, \tag{17}$$

$$\frac{\mathrm{d}s}{\mathrm{d}t} = 1 + sF, \quad \text{at } \xi = 1. \tag{18}$$

We now examine the behaviour of (15)–(18) as $t \to 0^+$. This will then give an initial condition which can be used in the numerical scheme. It is necessary to have a self-consistent asymptotic structure in this limit to ensure that the numerical scheme is second order convergent for $F, \frac{\partial F}{\partial \xi}$ and s. It also resolves the issues regarding the start-up of a computation for a region that initially has zero thickness. From (18) it is clear that $s = t$ as $t \to 0^+$ and in this limit (15)–(17) reduce to

$$F''(\xi) = 0, \quad F(0) = 0, \quad F'(1) = -(\lambda + 1), \tag{19}$$

which has solution

$$F = -(\lambda + 1)\xi. \tag{20}$$

We can now apply a finite difference scheme to (15)–(18); here we use the Keller box scheme described in [23,24], with the initial condition (20). When applying finite-difference schemes to moving-boundary problems it is common to use either a fully explicit scheme, or a semi-implicit scheme which treats F implicitly and s explicitly [5,15]. The resulting discretised system is then linear and therefore straightforward to solve. However, this imposes a severe restriction on the size of time-step that can be used in order that stability is maintained [15]. Whilst the semi-implicit scheme does not suffer from this constraint, it is formally only first-order accurate due to the explicit discretisation for s. The Keller box scheme [18,19] is a stable, second-order accurate finite-difference scheme, and is fully implicit since it involves two points at the new time level. It is also very compact as it only uses four neighbouring values in a box formulation. We note that Abd-El-Salam and Shehata [1] apply the implicit Crank–Nicolson discretisation to this model, using the same scaling as Cohen and Erneux [7], but it is less compact than the box scheme and will not give second order accuracy for the derivative variable.

Following [19] we consider a uniform mesh over the rectangle $0 \leqslant t \leqslant t_{max},\ 0 \leqslant \xi \leqslant 1$, with time step $\Delta t = t_{max}/N$ and spatial step $\Delta\xi = 1/I$ for a given N and I. Let U_i^n denote the numerical approximation of a variable u at $(\xi_i, t^n) := (i\Delta\xi, n\Delta t)$ for $i = 0, 1, \ldots, I$ and $n = 0, 1, \ldots, N$. On the mesh we define the finite difference operators for the variable U_i^n:

$$\mu_\xi U_{i+\frac{1}{2}}^{n+\frac{1}{2}} = \frac{U_{i+1}^{n+\frac{1}{2}} + U_i^{n+\frac{1}{2}}}{2}, \quad \delta_\xi U_{i+\frac{1}{2}}^{n+\frac{1}{2}} = \frac{U_{i+1}^{n+\frac{1}{2}} - U_i^{n+\frac{1}{2}}}{\Delta\xi}, \tag{21}$$

$$\mu_t U_{i+\frac{1}{2}}^{n+\frac{1}{2}} = \frac{U_{i+\frac{1}{2}}^{n+1} + U_{i+\frac{1}{2}}^{n}}{2}, \quad \delta_t U_{i+\frac{1}{2}}^{n+\frac{1}{2}} = \frac{U_{i+\frac{1}{2}}^{n+1} - U_{i+\frac{1}{2}}^{n}}{\Delta t}. \tag{22}$$

Then the box scheme consistently uses the operator $\mu_x \delta_t U_{i+\frac{1}{2}}^{n+\frac{1}{2}}$ to approximate U_t, $\mu_t \delta_x U_{i+\frac{1}{2}}^{n+\frac{1}{2}}$ to approximate U_x and $\mu_t \mu_x U_{i+\frac{1}{2}}^{n+\frac{1}{2}}$ to approximate U. It therefore necessary, as described in [18,23], to re-write (15) as a first-order system by setting $V = \frac{\partial F}{\partial \xi}$. Then the box scheme applied to (15) is given by

$$\mu_t \delta_\xi F_{i+\frac{1}{2}}^{n+\frac{1}{2}} = \mu_t \mu_\xi V_{i+\frac{1}{2}}^{n+\frac{1}{2}}, \tag{23}$$

$$\mu_t \delta_\xi V_{i+\frac{1}{2}}^{n+\frac{1}{2}} = (\mu_t s^{n+\frac{1}{2}})(\delta_t s^{n+\frac{1}{2}})\mu_\xi \mu_t F_{i+\frac{1}{2}}^{n+\frac{1}{2}} + \left(\mu_t s^{n+\frac{1}{2}}\right)^2 \mu_\xi \delta_t F_{i+\frac{1}{2}}^{n+\frac{1}{2}} - (\mu_\xi \xi_{i+\frac{1}{2}})(\mu_t s^{n+\frac{1}{2}})(\delta_t s^{n+\frac{1}{2}})\mu_\xi \mu_t V_{i+\frac{1}{2}}^{n+\frac{1}{2}}, \tag{24}$$

which holds for $i = 0, 1, \ldots, I-1$ and $n = 0, 1, \ldots, N-1$. The boundary condition (16) is simply $F_0^n = 1$ for $n = 0, 1, \ldots, N$, whilst boundary conditions (17) and (18) are discretised as

$$\left[\lambda + 1 + (\mu_t s^{n+\frac{1}{2}})\mu_t F_I^{n+\frac{1}{2}}\right](\delta_t s^{n+\frac{1}{2}}) = -\mu_t V_I^{n+\frac{1}{2}}, \tag{25}$$

$$\delta_t s^{n+\frac{1}{2}} = 1 + (\mu_t s^{n+\frac{1}{2}})\mu_t F_I^{n+\frac{1}{2}}. \tag{26}$$

We use (20) to give the initial conditions

$$F_i^0 = -(\lambda + 1)\xi_i, \quad V_i^0 = -(\lambda + 1), \quad \text{for } i = 0, 1, \ldots, I. \tag{27}$$

Eqs. (23) and (24) involve s^{n+1} and so it is necessary to solve a non-linear equation at each time-step. This is achieved by iterating on s, using its values at level n as a starting guess. For the classic Stefan problem, s can be updated using the Stefan condition until some desired tolerance, ε, is reached [23]. Denoting by $s^{n+1}_{(m)}$ the values for s^{n+1} after m iterations, the convergence criterion used is

$$\left| s^{n+1}_{(m+1)} - s^{n+1}_{(m)} \right| < \varepsilon. \tag{28}$$

For the problem considered here, we can use either (25) or (26) to update s. It is more convenient to iterate on (26), since rearranging (25) leads to a quadratic equation for s^{n+1}. Then (25) is used as the boundary condition at $\xi = 1$ which is solved with 23,24 and the boundary condition $F^n_0 = 1$ at each time-step.

It should be noted that we could have simply set $u(x,t) = F(\xi,t)$ in (14), as in [1], but in experiments to determine the convergence of the scheme it turns out that the convergence parameter approaches 2 much quicker for the transformation given in (14). This is due to the fact that the starting condition resulting from using $u(x,t) = F(\xi,t)$ is simply constant and this has been shown to give first order accuracy in a similar Stefan problem [22]. Results are not given here but experiments can be carried out in an identical manner to those discussed in [23,24], and second order convergence can be shown for F, V and s.

4. Small time asymptotic solution

Whilst we could perform an asymptotic analysis of the governing equations after immobilising the boundary [7], it is more convenient to consider (8)–(12) directly. We will see this explicitly when considering the large time expansion in Section 5 where it is necessary to analyse the original equations, rather than the transformed equations, to obtain higher order terms. In addition, the small time solution described in [7] uses the unknown moving boundary position as the expansion parameter which means they end up having to solve a non-linear equation to determine this parameter. The formulation described here avoids this complication.

Thus for $\lambda = \mathcal{O}(1)$ we set

$$t = \epsilon\tau, \quad x = \epsilon^a y, \quad s(t) = \epsilon^a L(\tau), \quad u(x,t) = \epsilon^b v(y,\tau), \tag{29}$$

where $\epsilon \ll 1$ is an artificial parameter [6,16] and $a, b \geqslant 0$. Then (8)–(11) reduce to

$$\epsilon^{2a-1}\frac{\partial v}{\partial \tau} = \frac{\partial^2 v}{\partial y^2}, \quad 0 < y < L(\tau) \tag{30}$$

$$\epsilon^b v = 1, \quad \text{at } y = 0 \tag{31}$$

$$(\lambda + \epsilon^b v)\epsilon^{a-1}\frac{\mathrm{d}L}{\mathrm{d}\tau} = -\epsilon^{b-a}\frac{\partial v}{\partial y}, \quad \text{at } y = L \tag{32}$$

$$\epsilon^{a-1}\frac{\mathrm{d}L}{\mathrm{d}\tau} = \epsilon^b v, \quad \text{at } y = L. \tag{33}$$

Anticipating a quasi steady balance in the PDE (31) at leading order, we scale to bring out the appropriate balances and to ensure that the final solution is independent of the artificial parameter ϵ. From (31) it follows that $b = 0$; this ensures a consistent boundary condition in the limit $\epsilon \to 0$. The condition (33) then determines $a = 1$; if we had chosen $a = 1/2$ to balance the PDE (31) then (33) would reduce to $\frac{\mathrm{d}L}{\mathrm{d}\tau} = 0$ in the limit $\epsilon \to 0$, and thus from the initial condition the front will not move at leading order. With $a = 1,\ b = 0$ Eqs. (30)–(33) become

$$\epsilon\frac{\partial v}{\partial \tau} = \frac{\partial^2 v}{\partial y^2}, \quad 0 < y < L(\tau), \tag{34}$$

$$v = 1, \quad \text{at } y = 0, \tag{35}$$

$$(\lambda + v)\epsilon\frac{\mathrm{d}L}{\mathrm{d}\tau} = -\frac{\partial v}{\partial y}, \quad \text{at } y = L(\tau), \tag{36}$$

$$\frac{\mathrm{d}L}{\mathrm{d}\tau} = v, \quad \text{at } y = L(\tau), \tag{37}$$

with $L(0) = 0$. We now expand v and L in terms of the small parameter ϵ by setting

$$v(y,\tau) = v_0(y,\tau) + \epsilon v_1(y,\tau) + \epsilon^2 v_2(y,\tau) + \mathcal{O}(\epsilon^3), \tag{38}$$

$$L(\tau) = L_0(\tau) + \epsilon L_1(\tau) + \epsilon^2 L_2(\tau) + \mathcal{O}(\epsilon^3). \tag{39}$$

The leading order problem is

$$\frac{\partial^2 v_0}{\partial y^2} = 0, \quad \text{with} \quad v_0(0,\tau) = 1, \quad \frac{\partial v_0}{\partial y}(L_0,\tau) = 0, \quad \frac{\mathrm{d}L_0}{\mathrm{d}\tau} = v_0(L_0,\tau),$$

which has solution

$$v_0 = 1, \quad L_0 = \tau. \tag{40}$$

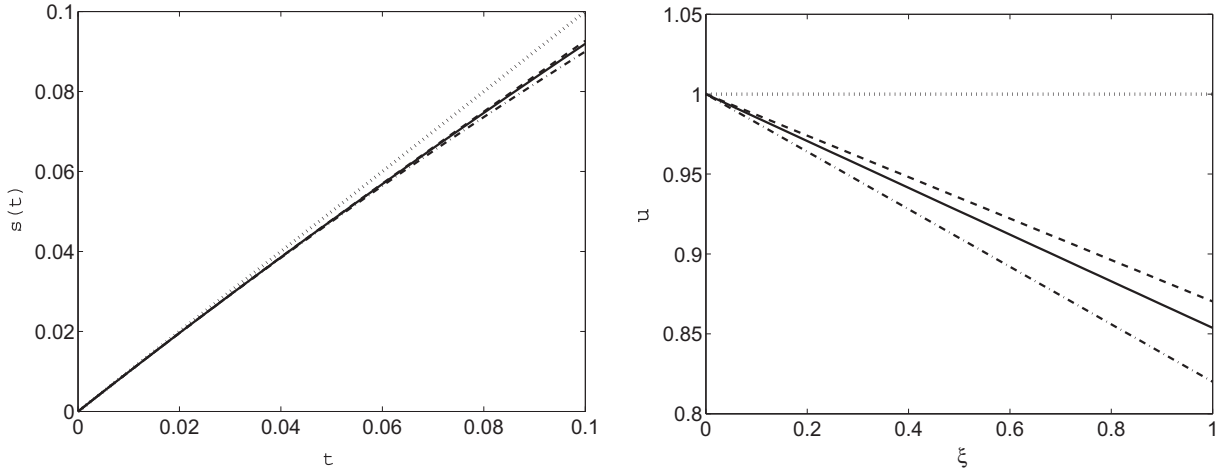

Fig. 1. Comparison of numerical (solid line) and the small time asymptotic solutions (dotted line denotes leading order, dot-dashed denotes first order and dashed denotes second order). Left plot shows s against t and right plot shows u against ξ (at $t = 0.1$) for $\lambda = 1$.

The $\mathcal{O}(\epsilon)$ terms also satisfy $\frac{\partial^2 v_1}{\partial y^2} = 0$ with $v_1(0,\tau) = 0$ and

$$[\lambda + v_0(L_0,\tau)]\frac{dL_0}{d\tau} = -L_1\frac{\partial^2 v_0}{\partial y^2}(L_0,\tau) - \frac{\partial v_1}{\partial y}(L_0,\tau), \tag{41}$$

$$\frac{dL_1}{d\tau} = L_1\frac{\partial v_0}{\partial y}(L_0,\tau) + v_1(L_0,\tau). \tag{42}$$

Note that these are obtained from a Taylor series expansion of the boundary conditions (36) and (37). The solution is

$$v_1 = -(\lambda+1)y, \quad L_1 = -\frac{1}{2}(\lambda+1)\tau^2. \tag{43}$$

Continuing the expansion it can be shown that the solution for the $\mathcal{O}(\epsilon^2)$ problem is

$$v_2 = (\lambda+1)(\lambda+2)\tau y, \quad L_2 = \frac{1}{6}(\lambda+1)(3\lambda+5)\tau^3, \tag{44}$$

and so back in the original variables we have

$$u = 1 - (\lambda+1)x + (\lambda+1)(\lambda+2)tx + \cdots, \tag{45}$$

$$s = t - \frac{1}{2}(\lambda+1)t^2 + \frac{1}{6}(\lambda+1)(3\lambda+5)t^3 + \cdots. \tag{46}$$

The first two terms were given in [7,12], but is only by considering the second order terms that we see the time dependence in u.

Figs. 1 and 2 compare the numerical solution with the small time asymptotic solutions for two different values of λ. We observe that including more terms in the asymptotic expansion leads to more accurate results, as expected. When $\lambda = 1$ the expansion for u holds for $t = 0.1$, and even for larger times, but as we increase λ it is only valid for smaller times. Also note that these results are consistent with the expansions in (45) and (46). For example, in the case shown in Fig. 1, the error between the numerical solution and the second order expansion at $t = 0.1$ is 1.7×10^{-2} for u and 7.1×10^{-4} for s. These are $\mathcal{O}(t^2)$ and $\mathcal{O}(t^4)$ respectively which correspond to the errors in each expansion.

5. Large time asymptotic solution

To consider the large time asymptotic solution we set (analogous to (29) with $\lambda = \mathcal{O}(1)$)

$$t = \frac{\tau}{\delta^2}, \quad x = \delta^a y, \quad s(t) = \delta^a L(\tau), \quad u(x,t) = \delta^b v(y,\tau), \tag{47}$$

where $\delta \ll 1$ is an artificial parameter and $a, b \leqslant 0$. We have chosen δ^2 in the time transformation to avoid having an expansion involving the square root of the small parameter. Here we do not expect quasi steady behaviour of the transformed PDE (8) and so we determine a from balancing this equation, leading to the choice $a = -1$. The transformed boundary condition (9) shows that $b = 0$, again to ensure consistency in the limit $\delta \to 0$, and so (8)–(11) reduce to

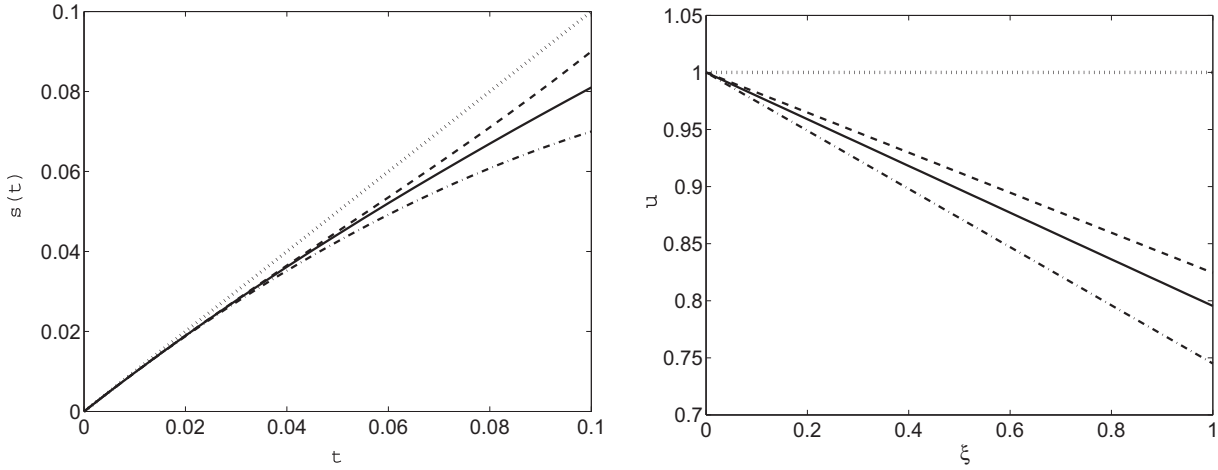

Fig. 2. Comparison of numerical (solid line) and the small time asymptotic solutions (dotted line denotes leading order, dot-dashed denotes first order and dashed denotes second order). Left plot shows s against t and right plot shows u against ξ (at $t = 0.05$) for $\lambda = 5$.

$$\frac{\partial v}{\partial \tau} = \frac{\partial^2 v}{\partial y^2}, \quad 0 < y < L(\tau), \tag{48}$$

$$v = 1, \quad \text{at } y = 0, \tag{49}$$

$$(\lambda + v)\frac{\mathrm{d}L}{\mathrm{d}\tau} = -\frac{\partial v}{\partial y}, \quad \text{at } y = L, \tag{50}$$

$$\delta\frac{\mathrm{d}L}{\mathrm{d}\tau} = v, \quad \text{at } y = L. \tag{51}$$

We now expand v and L in terms of the small parameter δ by setting

$$v(y,\tau) = v_0(y,\tau) + \delta v_1(y,\tau) + \delta^2 v_2(y,\tau) + \cdots, \tag{52}$$

$$L(\tau) = L_0(\tau) + \delta L_1(\tau) + \delta^2 L_2(\tau) + \cdots. \tag{53}$$

The leading order problem is

$$\frac{\partial v_0}{\partial \tau} = \frac{\partial^2 v_0}{\partial y^2}, \quad \text{with} \quad v_0(0,\tau) = 1, \quad [\lambda + v_0(L_0,\tau)]\frac{\mathrm{d}L_0}{\mathrm{d}\tau} = -\frac{\partial v_0}{\partial y}(L_0,\tau), \quad v_0(L_0,\tau) = 0. \tag{54}$$

At this stage it is convenient to introduce the similarity transformation

$$\eta = \frac{y}{2\sqrt{\tau}}, \quad v_i(y,\tau) = \tau^{c_i} f_i(\eta), \tag{55}$$

for $i = 0, 1, 2, \ldots$. Substituting for $i = 0$ into (54) we see immediately that $c_0 = 0$ and then the solution is

$$v_0 = 1 - \frac{\mathrm{erf}(y/[2\sqrt{\tau}])}{\mathrm{erf}(\alpha_0)}, \quad L_0 = 2\alpha_0\sqrt{\tau}, \tag{56}$$

where α_0 satisfies the transcendental equation

$$\lambda\alpha_0\sqrt{\pi}\,\mathrm{erf}(\alpha_0)e^{\alpha_0^2} = 1. \tag{57}$$

Cohen and Erneux [7] considered a large time analysis of the governing equations in the immobilised form, i.e. (15)–(18). Evans and King [12] also only quote the expansion up to this order. However, using this does not allow higher order terms to be determined. Here we see that the $\mathcal{O}(\delta)$ terms satisfy

$$\frac{\partial v_1}{\partial \tau} = \frac{\partial^2 v_1}{\partial y^2}, \tag{58}$$

with $v_1(0,\tau) = 0$ and

$$[\lambda + v_0(L_0,\tau)]\frac{\mathrm{d}L_1}{\mathrm{d}\tau} + \left[L_1\frac{\partial v_0}{\partial y}(L_0,\tau) + v_1(L_0,\tau)\right]\frac{\mathrm{d}L_0}{\mathrm{d}\tau} = -L_1\frac{\partial^2 v_0}{\partial y^2}(L_0,\tau) - \frac{\partial v_1}{\partial y}(L_0,\tau), \tag{59}$$

$$\frac{\mathrm{d}L_0}{\mathrm{d}\tau} = L_1\frac{\partial v_0}{\partial y}(L_0,\tau) + v_1(L_0,\tau). \tag{60}$$

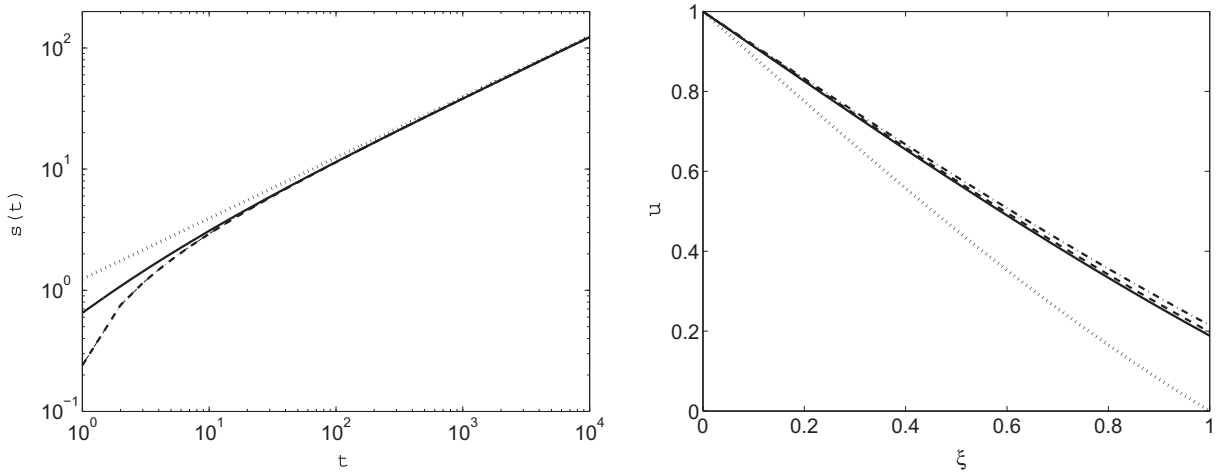

Fig. 3. Comparison of numerical (solid line) and the large time asymptotic solutions (dotted line denotes leading order, dot-dashed denotes first order and dashed denotes second order). Left plot shows s against t and right plot shows u against ξ (at $t = 10$) for $\lambda = 1$.

With the similarity transformation in (55) for $i = 1$, the PDE (58) reduces to

$$4c_1 f_1(\eta) - 2\eta f_1\prime(\eta) - f_1''(\eta) = 0. \tag{61}$$

To determine c_1 we examine the boundary conditions (59) and (60). Note that $y = L_0$ corresponds to $\eta = \alpha_0$ and so Eqs. (59) and (60) become

$$\lambda \frac{dL_1}{d\tau} + \left[-\frac{\lambda \alpha_0 L_1}{\sqrt{\tau}} + \tau^{c_1} f_1(\alpha_0) \right] \frac{\alpha_0}{\sqrt{\tau}} = -\frac{\lambda \alpha_0^2 L_1}{\tau} - \frac{1}{2}\tau^{c_1 - 1/2} f_1'(\alpha_0), \tag{62}$$

$$\frac{\alpha_0}{\sqrt{\tau}} = -\frac{\lambda \alpha_0 L_1}{\sqrt{\tau}} + \tau^{c_1} f_1(\lambda_0). \tag{63}$$

Thus $c_1 = -1/2$ and $L_1 = \alpha_1$ is constant. The general solution of (61) is then

$$f_1(\eta) = C_1 \operatorname{erfi}(\eta) e^{-\eta^2} + D_1 e^{-\eta^2}, \tag{64}$$

where $\operatorname{erfi}(x)$ is the imaginary error function, defined by $\operatorname{erfi}(x) \equiv -i \operatorname{erf}(ix)$. Eq. (64) must also satisfy $f_1(0) = 0$ (from $v_1(0, \tau) = 0$). Since $\operatorname{erfi}(0) = 0$ this requires $D_1 = 0$. We now use (62) and (63) to determine α_1 and C_1. Surprisingly, this turns out to simply yield $\alpha_1 = -1/\lambda$ and $C_1 = 0$, or $L_1 = -1/\lambda$ and $v_1 = 0$.

The $\mathcal{O}(\delta^2)$ solution can be determined in a similar way and we find that $L_2 = 0$ but now v_2 is non-zero and given by

$$v_2 = \frac{C_2 y}{2\tau^{3/2}} e^{-y^2/[4\tau]}, \quad C_2 = -\frac{\alpha_0}{2\lambda} e^{\alpha_0^2}. \tag{65}$$

Thus the first three terms in the series expansion can be written as

$$u \sim 1 - \frac{\operatorname{erf}(x/[2\sqrt{t}])}{\operatorname{erf}(\alpha_0)} + \frac{C_2 x}{2t^{3/2}} e^{-x^2/[4t]}, \qquad s \sim 2\alpha_0 \sqrt{t} - \frac{1}{\lambda}. \tag{66}$$

Evans and King [12] analyse a similar model when considering asymptotic results of the Stefan problem with undercooling. The only difference between their model and (8)–(12) is that they choose their length-scale differently so that λ multiplies s_t in the boundary condition (11). They only quote the first two terms in the large time expansion, and this agrees with (66), and suggest that the next term in the moving boundary position s is $\mathcal{O}(1/\sqrt{t})$. However, here we see that since L_2 is zero then the next term will in fact be $\mathcal{O}(1/t)$.

Figs. 3 and 4 compare the numerical solution with the large time asymptotic solutions for two different values of λ. Notice that the first and second order solutions are identical for s. Again we see that the higher order solution gives the best approximation, and this becomes even more noticeable as λ increases. The results for u show how important it is to include more than just the leading order terms in the solution, as this predicts $u = 0$ at $x = s$ (or $\xi = 1$) which is very inaccurate. Note that, in contrast to the small time asymptotic analysis, the Figures here show that the expansions for u are more accurate than for s. This is entirely consistent with the expansions in (66) because u and s are not to the same level of accuracy in t.

6. Large λ asymptotic solution

The parameter λ can be large [17] and so we now consider the large λ asymptotic limit. We also saw in Sections 4 and 5 that the small and large expansion break down as λ increases. We therefore define $\epsilon = 1/\lambda$ and re-scale Eqs. (8)–(12) using

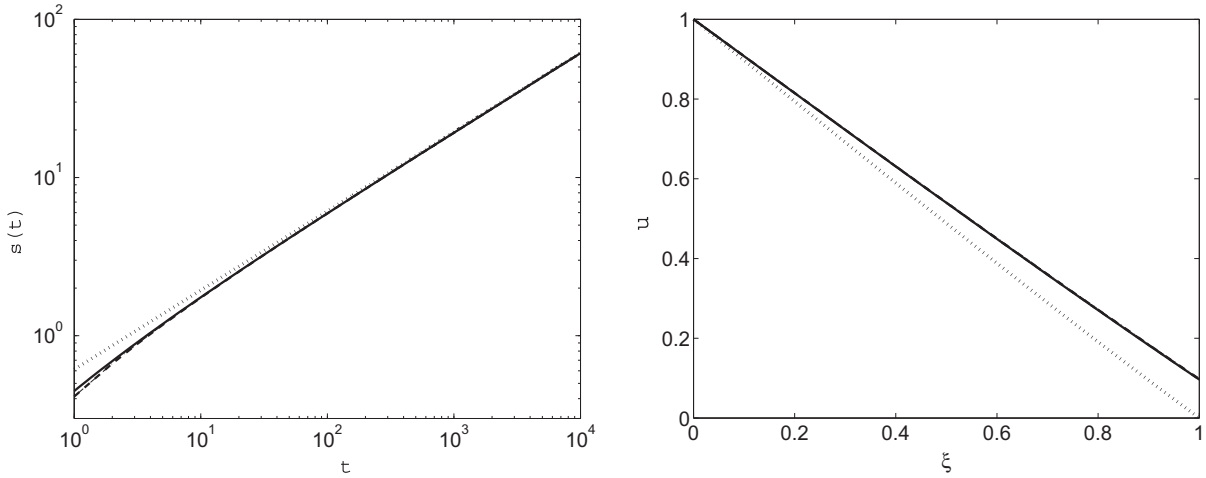

Fig. 4. Comparison of numerical (solid line) and the large time asymptotic solutions (dotted line denotes leading order, dot-dashed denotes first order and dashed denotes second order). Left plot shows s against t and right plot shows u against ξ (at $t = 10$) for $\lambda = 5$.

the definitions in (29) for $\epsilon \ll 1$. From the boundary conditions (9) and (11) it also follows that $b = 0,\ a = 1$ and so (1)–(4) become

$$\epsilon \frac{\partial v}{\partial \tau} = \frac{\partial^2 v}{\partial y^2}, \quad 0 < y < L(\tau), \tag{67}$$

$$v = 1, \quad \text{at } y = 0, \tag{68}$$

$$(1 + \epsilon v)\frac{\mathrm{d}L}{\mathrm{d}\tau} = -\frac{\partial v}{\partial y}, \quad \text{at } y = L, \tag{69}$$

$$\frac{\mathrm{d}L}{\mathrm{d}\tau} = v, \quad \text{at } y = L, \tag{70}$$

with $L(0) = 0$. Expanding v and L in terms of ϵ, as in (38) and (39), gives the leading order problem

$$\frac{\partial^2 v_0}{\partial y^2} = 0, \quad \text{with} \quad v_0(0,\tau) = 1, \quad \frac{\mathrm{d}L_0}{\mathrm{d}\tau} = -\frac{\partial v_0}{\partial y}(L_0,\tau), \quad \frac{\mathrm{d}L_0}{\mathrm{d}\tau} = v_0(L_0,\tau),$$

which has solution

$$v_0 = 1 - \frac{y}{\sqrt{1+2\tau}}, \quad L_0 = -1 + \sqrt{1+2\tau}. \tag{71}$$

It is straightforward to determine the $\mathcal{O}(\epsilon)$ and $\mathcal{O}(\epsilon^2)$ solutions, again with the boundary conditions expanded using a Taylor series, as discussed in Section 4 and Section 5. We find that

$$\begin{aligned} v = 1 &- \frac{y}{\sqrt{1+2\tau}} + \epsilon\left(\frac{y^3}{6(1+2\tau)^{3/2}} - \frac{y}{3\sqrt{1+2\tau}} - \frac{2y}{3(1+2\tau)^2}\right) \\ &+ \epsilon^2\left(-\frac{y^5}{40(1+2\tau)^{5/2}} + \frac{y^3}{18(1+2\tau)^{3/2}} + \frac{4y^3}{9(1+2\tau)^3} + \frac{(22\tau^3+33\tau^2+84\tau-26)y}{45(1+2\tau)^{7/2}} - \frac{2(10\tau-13)y}{45(1+2\tau)^3}\right) + \mathcal{O}(\epsilon^3) \end{aligned} \tag{72}$$

$$L = -1 + \sqrt{1+2\tau} + \epsilon\left(\frac{1-\tau}{3\sqrt{1+2\tau}} - \frac{1}{3(1+2\tau)}\right) + \epsilon^2\left(\frac{19-10\tau}{45(1+2\tau)^2} + \frac{46\tau^3+39\tau^2-18\tau-38}{90(1+2\tau)^{5/2}}\right) + \mathcal{O}(\epsilon^3). \tag{73}$$

Then $u(x,t)$ and $s(t)$ are determined from the transformations $t = \epsilon\tau,\ x = \epsilon y,\ s = \epsilon L$ and $u = v$.

The first two terms were quoted in [12] where they compared the leading order and $\mathcal{O}(\epsilon)$ solutions for the moving boundary position s with a numerical solution. They showed that very good agreement could be reached even down to $\lambda = 1$. In Fig. 5 we show results for both L and v for $\lambda = 2$ and $\lambda = 5$. Again we can see that the expansion becomes more accurate as we include more terms in the expansion. Once λ becomes larger than 2 it is difficult to see any difference between the numerical and first and second order solutions, though even when $\lambda = 10$ there is a noticeable difference between these solutions and the leading order term.

It should be noted that the number of iterations required to fulfil (28) was found to increase dramatically for large values of λ. A more robust strategy came from using a non-linear solver, such as fzero in Matlab, at each time-step to determine the position of the moving front at level $n+1$ [22].

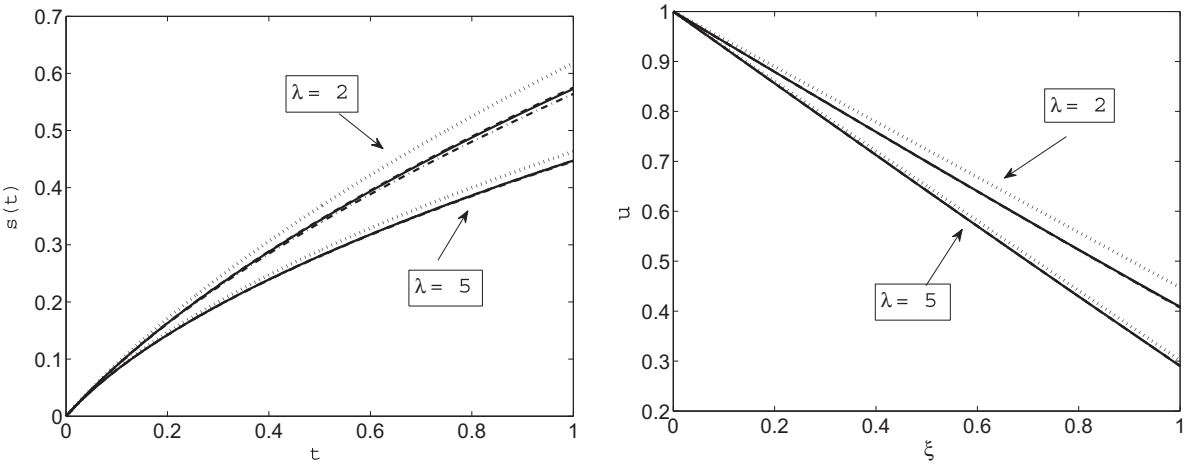

Fig. 5. Comparison of numerical (solid line) and the large lambda asymptotic solutions (dotted line denotes leading order, dot-dashed denotes first order and dashed denotes second order). Left plot shows L against τ and right plot shows v against ξ (at $\tau = 1$) for $\lambda = 2$ and $\lambda = 5$.

7. The combined integral method (CIM)

In this section we describe how the heat balance integral method (HBIM) can be applied to the system (8)–(12). The purpose is twofold, firstly to validate the numerical and asymptotic solutions described above, and secondly to highlight an accurate solution method which is valid for all times and all parameter values. The HBIM is a well-known method for finding approximate solutions to thermal problems, see [14,20] and references therein. It has proved particularly valuable in the solution of Stefan problems, where few analytical solutions exist. The popularity of the HBIM is due primarily to its simplicity. However, the method has various well-known drawbacks [20,25,26]. For example, the choice of approximating function is arbitrary and this is key to the method's accuracy. To compound the ambiguity there are often different ways to formulate even the most basic problem, and this also affects the accuracy [20]. An extension to the HBIM, known as the Refined Integral method (RIM) [20,28], simply involves integrating the heat equation twice. For certain situations the RIM can improve on the HBIM, but there is no set rule on as to which will be the best method. The relative merits of each method are discussed in [20].

To apply these integral methods we approximate the concentration with the polynomial form

$$u(x,t) = a + b\left(1 - \frac{x}{s}\right) + c\left(1 - \frac{x}{s}\right)^m, \tag{74}$$

where a, b, c are possibly time dependent and $m > 1$. For the classic HBIM and RIM this would be specified, usually setting $m = 2$. In the approach adopted by Mitchell and Myers [21,27] the exponent m is left unknown and determined as part of the solution process. The HBIM and RIM are combined to give the extra equation to determine m. This is known as the *combined integral method* (CIM) and is now applied to Eqs. (8)–(12).

Two of the coefficients in (74) can be eliminated by applying boundary condition (9) and the combination of (10) and (11). Then we find

$$u(x,t) = a + s(\lambda + a)a\left(1 - \frac{x}{s}\right) + [1 - a - s(\lambda + a)a]\left(1 - \frac{x}{s}\right)^m. \tag{75}$$

For the HBIM the heat equation is integrated over $x \in [0, s]$ to give (after applying the Leibniz rule)

$$\frac{\mathrm{d}}{\mathrm{d}t}\int_0^s u\,\mathrm{d}x - u|_{x=s}\frac{\mathrm{d}s}{\mathrm{d}t} = \left.\frac{\partial u}{\partial x}\right|_{x=s} - \left.\frac{\partial u}{\partial x}\right|_{x=0}. \tag{76}$$

The RIM is derived from integrating the heat equation twice over the spatial domain. There is a choice between taking the first integral over $x \in [0, \xi]$ or $[\xi, s]$ and then taking the second for $\xi \in [0, s]$. These lead to two possible formulations which exhibit different levels of accuracy [20,27]. However, since the CIM combines both the HBIM and RIM formulations are combined, it turns out that this particular ambiguity is removed. Here we quote the formulation which requires one integration instead of two, namely

$$\frac{\mathrm{d}}{\mathrm{d}t}\int_0^s xu\,\mathrm{d}x - su|_{x=s}\frac{\mathrm{d}s}{\mathrm{d}t} = s\left.\frac{\partial u}{\partial x}\right|_{x=s} - u|_{x=s} + u|_{x=0}. \tag{77}$$

We must also satisfy the boundary condition (11), and using (75) with $x = s$ this reduces to

$$\frac{\mathrm{d}s}{\mathrm{d}t} = a. \tag{78}$$

The ODEs (76)–(78) are now used to determine the three unknowns s, a and m.

Substituting (75) into (76) leads to the expression

$$s\left[m+\frac{1}{2}(m-1)s(\lambda+2a)\right]\frac{da}{dt}+[(m-1)s(\lambda+a)a+1-a]\frac{ds}{dt}-\frac{s[1-a-s(\lambda+a)a]}{m+1}\frac{dm}{dt}$$
$$=\frac{m(m+1)}{s}[1-a-s(\lambda+a)a], \tag{79}$$

whilst (77) becomes

$$s\left[\frac{1}{2}m(m+3)+\frac{1}{6}(m+4)(m-1)s(\lambda+2a)\right]\frac{da}{dt}+\left[\frac{1}{2}(m+4)(m-1)s(\lambda+a)a+2(1-a)\right]\frac{ds}{dt}$$
$$-\frac{(2m+3)s[1-a-s(\lambda+a)a]}{(m+1)(m+2)}\frac{dm}{dt}=\frac{(m+1)(m+2)}{s}[1-a-s(\lambda+a)a]. \tag{80}$$

The HBIM and RIM formulations simply involve specifying m, typically $m=2$ to give a quadratic profile in (75), and then solving either (79) or (80) respectively, along with the equation $a=s_t$. Of course a could be eliminated to give a second order equation for s. Either way, an extra initial condition need to be specified. We are given that $s(0)=0$ and from comparing the small time asymptotic solution (45)–(75) we conclude that $a(0)=1$. To apply the CIM, we combine (79) and (80) with $a=s_t$ and solve for a, s and m. This requires finding $m(0)$ which is not so straightforward. Mitchell & Myers [21,27] used a small time analysis of the ODEs to determine $m(0)$ but it seems that this is not possible here. If we assume $m(0)=m_0\neq 0$ and set $s\sim t+s_1t^2$, therefore giving $a\sim 1+2s_1t$, then from both equations it follows that $s_1=-(\lambda+1)/2$. This is precisely the small time solution, and if we continue the expansion we find that both the HBIM and CIM give the asymptotic solution in this limit, for any value of m_0.

Preliminary numerical experiments, implemented with the ODE solver ode15s in Matlab, suggest that $m_0=2$ which is independent of λ, and also that m quickly tends to a steady-state value. The solver is not robust to large values of λ, where m quickly becomes negative which is not physically realistic. We would like to be able to find a constant value of m which can be used for all t (and a large range of λ values).

To this end we consider a large time expansion of (79) and (80). We assume that $m\equiv m_\infty$ is constant and $s=2\alpha\sqrt{t}$, which is motivated by the large time expansion of the original system given in Section 5. Then $a=\alpha/\sqrt{t}, da/dt=-\alpha/[2\sqrt{t^3}]$ and the leading order terms in (79) and (80) satisfy

$$[(m_\infty-1)\lambda\alpha^2+1]\alpha=\frac{m_\infty(m_\infty+1)}{2\alpha}(1-2\lambda\alpha^2), \tag{81}$$
$$\left[\frac{2}{3}(m_\infty+4)(m_\infty-1)\lambda\alpha^2+2\right]\alpha=\frac{(m_\infty+1)(m_\infty+2)}{2\alpha}(1-2\lambda\alpha^2). \tag{82}$$

This pair of equations can be solved to determine α and m_∞. Then we can simply use the HBIM with this value of m_∞, instead of the more complicated CIM. The left plot in Fig. 6 shows m_∞ against λ and the right plot shows α against λ. We have also included the large time asymptotic value of α_0 from (57) in the right plot for comparison. Finally, Fig. 7 shows the HBIM solution, using m_∞ from solving (81) and (82), compared with the numerical solution for three values of λ. The solutions are virtually indistinguishable and so we conclude that for this problem the HBIM gives a very accurate representation of the solution for all parameter values and for a large range of times, and therefore validates our numerical and asymptotic

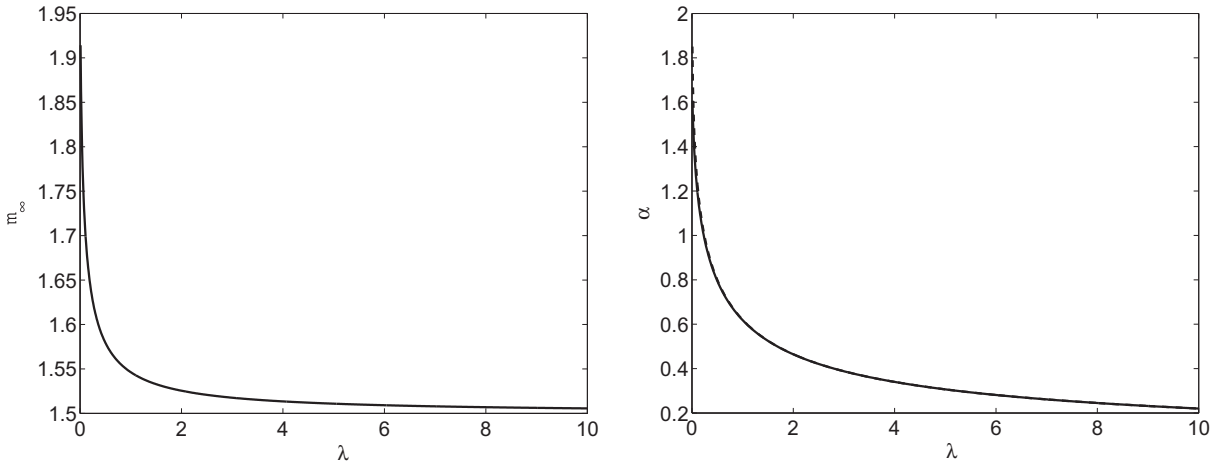

Fig. 6. The left plot shows m_∞ against λ and the right plot shows the CIM α against λ (solid) and the large time asymptotic α_0 against λ (dashed).

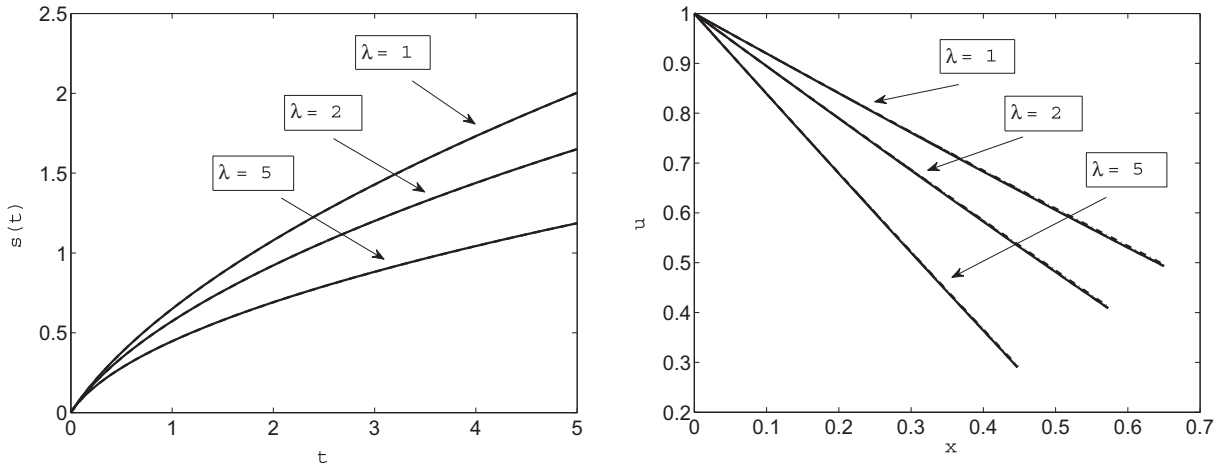

Fig. 7. Problem A with $\alpha = 0.2, \alpha = 1$ and $\alpha = 5$: Comparison of the numerical (solid line), the HBIM solution (dashed) using m_∞ and the HBIM solution (dot-dashed) using $m = 2$. Left plot shows s against t and right plot shows u against x (at $t = 1$).

solutions. We have also plotted the HBIM solution using the traditional value $m = 2$ and although there is not much difference it is clear that using m_∞ gives more accurate results.

8. Conclusions

In this paper we have considered asymptotic, numerical and approximate techniques for the one-dimensional free boundary problem (8)–(12) which arises in the diffusion of glassy polymers. We provide an accurate numerical scheme which is also easy to implement, and a complete asymptotic analysis in the limits $t \to 0^+, t \to \infty$ and $\lambda \to \infty$. It should also be highlighted that analysing the equations in their original form, rather than first immobilising the boundary, leads to a systematic approach which can be applied for all the limiting expansions. In the small time expansion we did not need to use the unknown moving position variable as the expansion parameter, and for the large time expansion we were able to determine higher order terms that did not inaccurately predict a zero concentration at the phase-change position [8,12]. Most previous work concentrates on results for s but we have also shown results for u, which is the variable that most emphasizes this issue.

In addition, our application of the HBIM to this problem has not previously been attempted by other authors. We have described in detail how to implement the method for the problem (8)–(12) and have showed how it gives very accurate results for all times and for a large range of values of the control parameter λ. We also considered a variant on the HBIM, called the CIM, which assumes the exponent in the concentration approximation is time dependent and determines this as part of the solution process. Preliminary numerical experiments showed that the ODEs could be difficult to handle and this led to developing a new and simpler strategy to find this exponent, by analysing the resulting ODEs in the limit as $t \to \infty$ to give a steady-state value which could then be used in the HBIM.

Future extensions include applying these methods to related problems where the polymer is exposed initially to a finite amount of penetrant [7,8]. Different behaviour arises depending whether the initial position of the moving front is zero or non-zero. A constant concentration is no longer maintained at $x = 0$, instead a zero flux is imposed there, and the system may approach an equilibrium value. This leads to a solution structure which is more complex than that described in this paper and it would be interesting to apply the techniques considered here to these models. The HBIM also has difficulties in dealing with zero flux boundary conditions; this is also evident in the related free boundary problem describing the diffusion of oxygen in absorbing tissue [11]. Resolving these issues would therefore be useful in several applications of non-linear moving boundary problems.

Acknowledgements

The authors acknowledge the support of MACSI, the Mathematics Applications Consortium for Science and Industry (www.macsi.ul.ie), funded by the Science Foundation Ireland Mathematics Initiative Grant 06/MI/005.

References

[1] M.R. Abd-El-Salam, M.H. Shehata, Coordinate transformation and implicit time discretization for diffusion in glassy polymers, Appl. Math. Comp. 113 (2000).
[2] D. Andreucci, R. Ricci, A free boundary problem arising from sorption of solvents in glassy polymers, Quarterly Appl. Math. 44 (4) (1987) 649–657.
[3] D.Y. Arifin, L.Y. Lee, C-H. Wang, Mathematical modeling and simulation of drug release from microspheres: Implications to drug delivery systems, Adv. Drug Delivery Rev. 58 (2006) 1274–1325.

[4] G. Astarita, G.C. Sarti, A class of mathematical models for sorption of swelling solvents in glassy polymers, Polymer Eng. Sci. 18 (5) (1978) 388–395.
[5] J. Caldwell, Y.Y. Kwan, Numerical methods for one-dimensional stefan problems, Commun. Numer. Methods Eng. 20 (2004) 535–545.
[6] I.E. Chang, Navier-stokes solutions at large distances from a finite body, J. Math. Mech. 10 (1961) 811–876.
[7] D.S. Cohen, T. Erneux, Free boundary problems in controlled release pharmaceuticals I: Diffusion in glassy polymers, SIAM J. Appl. Math. 48 (6) (1988) 1451–1465.
[8] D.S. Cohen, C. Goodhart, Sorption of a finite amount of swelling solvent in a glassy polymer, J. Polymer Sci. Polymer Phys. Edn. 25 (1987) 611–671.
[9] J. Crank, The Mathematics of Diffusion, Oxford University Press, Oxford, U.K., 1956.
[10] J. Crank, Free and Moving Boundary Problems, Oxford University Press, New York, 1984.
[11] J. Crank, R.S. Gupta, A moving boundary problem arising from the diffusion of oxygen in absorbing tissue, J. Inst. Math. Appl. 10 (1971) 19–33.
[12] J.D. Evans, J.R. King, Asymptotic results for the Stefan problem with kinetic undercooling, Quarterly J. Mech. Appl. Math. 53 (3) (2000) 449–473.
[13] A. Fasano, G.H. Meyer, M. Primicerio, On a problem in the polymer industry: theoretical and numerical investigation of swelling, SIAM J. Math. Anal. 17 (4) (1986) 945–960.
[14] T.R. Goodman, The heat-balance integral and its application to problems involving a change of phase, Trans. ASME 80 (1958) 335–342.
[15] S. Kutluay, A.R. Bahadir, A. Ozdes, The numerical solution of one-phase classical Stefan problem, J. Comput. Appl. Math. 81 (1997) 135–144.
[16] P.A. Lagerstrom, R.G. Casten, Basic concepts underlying singular perturbation techniques, SIAM Rev. 14 (1) (1972) 63–120.
[17] S.W. McCue, M. Hsieh, T.J. Morony, M.I. Nelson, Asymptotic and numerical results for a model of solvent-dependent drug diffusion through polymeric spheres, SIAM J. Appl. Math. 71 (6) (2011) 2287–2311.
[18] P.C. Meek, J. Norbury, Nonlinear moving boundary problems and a Keller box scheme, SIAM J. Numer. Anal. 21 (5) (1984) 883–893.
[19] S.L. Mitchell, K.W. Morton, A. Spence, Analysis of box schemes for reactive flow problems, SIAM J. Sci. Comput. 27 (4) (2006) 1202–1223.
[20] S.L. Mitchell, T.G. Myers, Application of standard and refined heat balance integral methods to one-dimensional Stefan problems, SIAM Rev. 52 (1) (2010) 57–86.
[21] S.L. Mitchell, T.G. Myers, Improving the accuracy of heat balance integral methods applied to thermal problems with time dependent boundary conditions, Int. J. Heat Mass Trans. 53 (2010) 3540–3551.
[22] S.L. Mitchell, M. Vynnycky, An accurate finite-difference method for ablation-type stefan problems, J. Comput. Appl. Math. 236 (2012) 4181–4192.
[23] S.L. Mitchell, M. Vynnycky, Finite-difference methods with increased accuracy and correct initialization for one-dimensional Stefan problems, App. Math. Comp. 215 (2009).
[24] S.L. Mitchell, M. Vynnycky, I.G. Gusev, S.S. Sazhin, An accurate numerical solution for the transient heating of an evaporating droplet, App. Math. Comput. 217 (2011).
[25] T.G. Myers, Optimizing the exponent in the heat balance and refined integral methods, Int. Commun. Heat Mass Trans. 36 (2) (2009) 143–147.
[26] T.G. Myers, Optimal exponent heat balance and refined integral methods applied to Stefan problems, Int. J. Heat Mass Trans. 53 (2010) 1119–1127.
[27] T.G. Myers, S.L. Mitchell, Application of the combined integral method to Stefan problems, Appl. Math. Model. 35 (2011) 4281–4294.
[28] N. Sadoun, E-K. Si-Ahmed, P. Colinet, On the refined integral method for the one-phase Stefan problem with time-dependent boundary conditions, App. Math. Model. 30 (2006).